ORGANIC CHEMISTRY FRONTIERS

CCS 中国化学会 CHINESE CHEMICAL SOCIETY

SIOC

ROYAL SOCIETY OF CHEMISTRY

Superfast and Highly Selective Water Transport by Hybrid Aquapentamers Incorporating a Non-Helicity Codon

Journal:	*Organic Chemistry Frontiers*
Manuscript ID	QO-RES-11-2024-002231.R1
Article Type:	Research Article
Date Submitted by the Author:	03-Jan-2025
Complete List of Authors:	Cao, Gaiping; Fuzhou University, College of Chemistry Yang, Zihong; Fuzhou University, College of Chemistry Zhao, Huaiqing; University of Jinan, School of Chemistry and Chemical Engineering Shen, Jie; Fuzhou University, College of Chemistry Chang, Wenju; Fuzhou University, College of Chemistry Liu, Zhiwei; Rowan University Zeng, Huaqiang; Fuzhou University, College of Chemistry

ARTICLE

Superfast and Highly Selective Water Transport by Hybrid Aquapentamers Incorporating a Non-Helicity Codon

Received 00th January 20xx,
Accepted 00th January 20xx

DOI: 10.1039/x0xx00000x

Gaiping Cao,[a] Zihong Yang,[a] Huaiqing Zhao,[b] Jie Shen,[a] Wenju Chang,*[a] Zhiwei Liu,*[b] and Huaqiang Zeng*[a]

H-bonded helically folded aromatic foldamers rely on the precise formation of H-bonds between each helicity codon and its neighboring codons to maintain their structure. We report here for the first time that the phenyl group, referred to as a non-helicity codon due to its inability to form H-bonds, does not necessarily disrupt the helical structure. Specifically, we modified our recently reported pyridine-based aquapentamers by sequentially replacing each of the five pyridine residues with a phenyl group, creating a series of five hybrid pentamers. The phenyl groups, unable to form H-bonds with the adjacent N-H bonds of the amides, introduce H-bond defects along the helical backbone. Despite these defects, three out of five pentamers still adopt a helical structure and function as highly selective and ultra-fast abiotic water channels, with the most efficient channel achieving a water transport rate of 1.8×10^9 H_2O s^{-1} per channel—approximately 30% of aquaporin Z's capacity.

Introduction

Over 4 billion people face significant water scarcity,[1, 2] making the demand for clean water one of the most pressing global challenges.[3, 4] Reverse osmosis (RO) has emerged as the primary technique for producing potable water, generating approximately 100 million tons of desalinated water daily from the oceans, the largest source of freshwater on Earth.[5-7] However, the significant energy requirements and substantial costs associated with this process hinder its widespread adoption.

Aquaporins (Aqps) are a unique class of protein-based membrane channels that facilitate ultra-fast water transport across lipid membranes while completely excluding salts and protons.[8-10] Specifically, Aquaporin Z (AqpZ) achieves a remarkable water transport rate of approximately 6×10^9 H_2O s^{-1} per channel,[11, 12] generating considerable interest in developing AqpZ-based membranes for low-energy filtration applications in fields such as kidney dialysis, as well as in industrial and municipal desalination projects.[13-20] Despite their impressive performance, Aqps face several limitations, including sensitivity to temperature and pH changes, potential denaturation under harsh conditions,[14] and challenges associated with large-scale production and functional reconstitution in membrane systems. These challenges underscore the need for alternative artificial water channels (AWCs) to replicate the key properties of AqpZ while addressing its limitations.

To be viable for practical water desalination applications, AWCs must achieve water transport permeability and selectivity comparable to the high performance of AqpZ. Despite the development of various types of AWCs over the past two decades,[12, 14, 20-49] achieving artificial water channels with both ultra-fast water transport capabilities and high rejection for NaCl and KCl remains a significant challenge.[32, 33, 42, 46, 50]

Utilizing a "sticky" end-mediated construction strategy,[51] we recently developed an aquafoldamer-based AWC **A** (Fig. 1a,b).[16, 33] Channel **A** exhibits water transport capability of 3×10^9 H_2O s^{-1} per channel, a value that is about 50% of the transport efficiency of AqpZ. With an internal hollow cavity of approximately 2.8 Å, which prevents the dehydration of hydrated ions, channel **A** also demonstrates high rejection of salts such as NaCl and KCl. Our findings indicate that an increased degree in freedom of water molecules and a reduced deviation from the optimal H-bonded structure, both resulting from an enlarged pore, are more influential than the slightly reduced wettability of the interior surface[52] in enhancing **A**-mediated water transport. Prompted by these findings, we are interested in further exploring the effects on the H-bonding network, the water transport rate and the helicity-forming tendency by selectively replacing a single helicity codon (e.g., a pyridine building block capable of forming intramolecular H-bonds, Fig. 1c) in **A** with a non-helicity codon (e.g., a phenyl group) that lacks this ability.

Here, we demonstrate that the presence of a single phenyl group—a non-helicity codon incapable of forming hydrogen bonds—often preserves the helical structure, as confirmed by crystal structures. Interestingly, within this series of five non-helicity-containing pentamers (**1**–**5**), the proton-transporting ability decreases in the order: **1** > **2** > **3** > **4** > **5**. This trend largely aligns with their water-transporting activities (**1** > **3** > **2** > **4** > **5**). Notably, the top performer, hybrid pentamer **1**, achieves a remarkable water transport efficiency

[a] College of Chemistry, Fuzhou University, Fuzhou, Fujian 350108, China. E-mail: wenjuchang@fzu.edu.cn; hqzeng@fzu.edu.cn.
[b] Department of Chemistry & Biochemistry, Rowan University, Glassboro, NJ 08028 USA. E-mail: liuz@rowan.edu.

Supplementary Information available: [details of any supplementary information available should be included here]. See DOI: 10.1039/x0xx00000x

of 1.8×10^9 H_2O s^{-1} per channel, representing 30% of AqpZ's capacity, while maintaining high rejection rates for both NaCl and KCl.

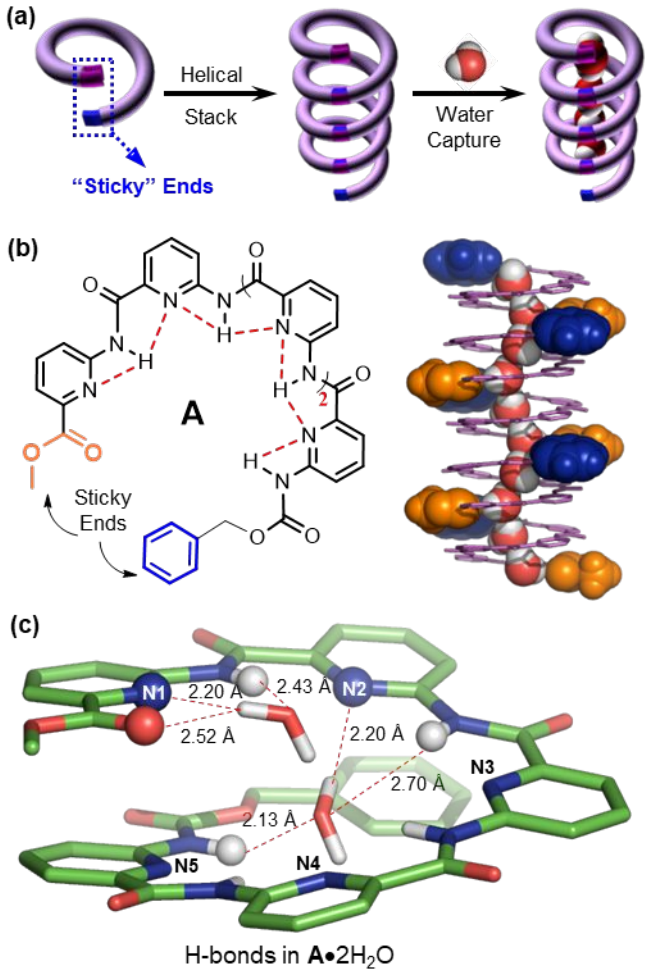

Fig.1 Molecular design and crystal structure of aquafoldamer **A**. (a) A "sticky" end-mediated molecular strategy for creating self-assembled 1D nanotubes for water recognition and transport. (b) Chemical and crystal structures of **A**, featuring "sticky" end-induced water-containing helically stacked configuration of $(\mathbf{A}\bullet 2H_2O)_5$. (c) H-bonds formed between the interior functional groups of **A** and the water pair.

Results and Discussion

Molecular Design and structural features of Partially H-bonded Aquafoldamers

As early as 2012,[51] we introduced a sticky end-mediated strategy for constructing one-dimensional (1D) nanotubes (Fig. 1a). In this approach, the helical ends of pentamer **A** are designed to feature a partially negatively charged oxygen atom and a partially positively charged hydrogen atom (Fig. 1b), enabling the formation of intermolecular hydrogen bonds with the corresponding hydrogen and oxygen atoms of another molecule **A**.[33] Within **A**, a continuous H-bonding network involving the pyridine N-atoms and amide H-atoms provides the driving force that induces the aromatic backbone to fold into a helical configuration (Fig. 1b). The enclose pore size of approximately 2.8 Å, which closely matches the size of a water molecule, facilitates exceptionally fast transmembrane water transport (3×10^9 H_2O s^{-1} per channel).

A detailed analysis of its water-containing structure reveals six strong intermolecular H-bonds between the water pair and the interior functional groups of **A** (Fig. 1c). These include one ester O-atom, two pyridine N-atoms and three amide H-atoms.

This raises the question: what would happen if we partially relaxed the fully hydrogen-bonded, rigid helical structure by replacing one of the five pyridine codons in A with a phenyl group, a non-helicity codon? Would this simple substitution, introducing an internal H-bond defect, disrupt the helical structure and thereby hinder the otherwise superfast water transport across the channel? Furthermore, how would the position of this substitution affect the structure and the water/proton transport functions?

To address these questions, we designed and synthesized hybrid pentamers **1**–**5** (Fig. 2a and Schemes S1–S2), incorporating sequential substitutions of the pyridyl unit with a phenyl unit, starting from the ester end of pentamer **A**.

The crystal structure reveals that pentamer **1** can self-assemble into one-dimensional structures through its "sticky" ends (Fig. 2c), forming a pore size slightly smaller than that of **A**. In this case, the H-atoms in the phenyl groups have a negligible effect on the pore size. In contrast, for pentamer **2**, steric hindrance from the hydrogen atoms in the phenyl groups leads to a significant reduction in pore size, decreasing to approximately 2.2 Å (Fig. 2d) that represents an ~20% reduction compared to **A**. Interestingly, pentamer **5** does not form a perfectly one-dimensional stacked structure through the "sticky" ends like **1** and **2**. Instead, it self-assembles via π-π stacking with adjacent molecules, resulting in the absence of well-defined channels perpendicular to the molecular plane (Fig. 2e). For **3** and **4**, we were unable to obtain good single crystals suitable for X-ray analysis.

It is interesting note that 1D nanotubes formed by **A**, **1**, **2** and **5** host well-organized chains of H_2O, CH_2Cl_2, MeOH and H_2O, respectively.

Superfast Transmembrane Water Transport by Pentamer 1

We quantitatively evaluated the water transport properties of **1**-**5** using a stopped-flow instrument, which enables precise measurement of rapid kinetics on a millisecond timescale to determine cross-membrane water permeability. Given the crystallographically determined helical height of approximately 5 Å for pentamers **1**, **2**, and **5** and the hydrophobic thickness of 28 Å for DOPC membranes,[53] it is estimated that around six molecules are required to fully span the hydrophobic region of the DOPC membrane.

We mixed DOPC lipids with **1**-**5** at molar ratios ranging from 500:1 to 900:1 in chloroform, resulting in lipid/channel molar ratios of 3000:1 to 5400:1. These mixtures were then used to prepare large unilamellar vesicles (LUVs) in a HEPES buffer (10 mM HEPES, 100 mM NaCl, pH 7.0). When these LUVs were exposed to an equal volume of a hypertonic 300 mM sucrose solution in the same buffer, water efflux occurred, leading to vesicle shrinkage and an increase in light scattering intensity (Fig. 3a). By analyzing the changes in light scattering over time, we extracted the water permeability (P_f in cm/s) of the vesicles with and without the water channels. Further factoring in channel insertion efficiency and the actual lipid concentration after extrusion (Figs. S5-S7 and Table S1), we calculated the single-channel permeability (P_w in cm^3/s) for **1**-**5** as summarized in Fig 3b.

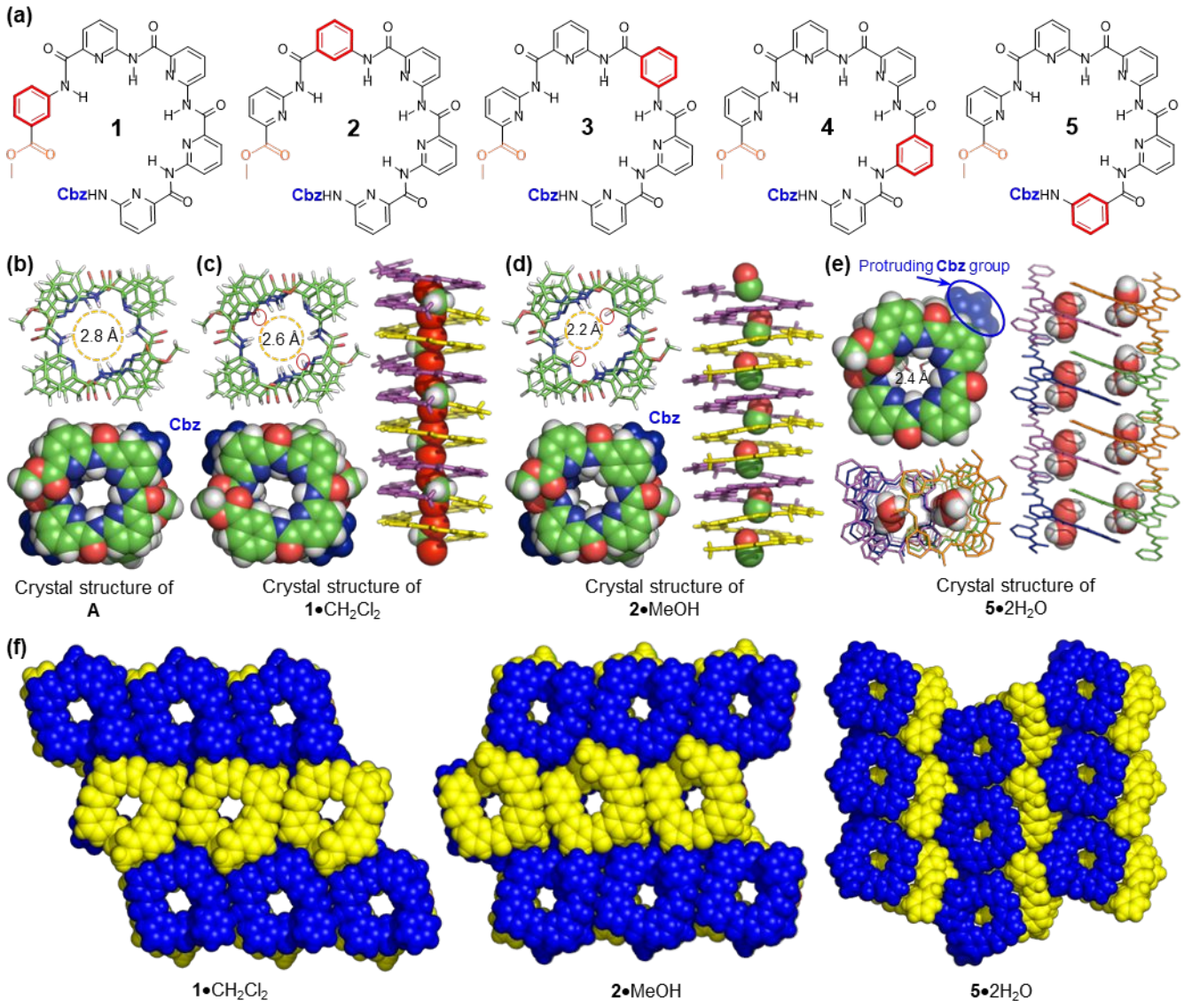

Fig.2 Molecular design of hybrid aquapentamers **1**-**5** that incorporate a non-helicity codon and their crystal structures. (a) Chemical structures of **1**-**5** having a phenyl unit at different positions. (b) Crystal structures of **A**. (c) - (e) Crystal structures of **1**, **2** and **5**. (f) The 2D crystal packing by **1**, **2** and **5**.

Our experimental results show that when a single pyridyl unit in **A** is replaced with a phenyl unit, the resulting hybrid pentamers continue to exhibit superfast transmembrane water transport, with **1** showing the highest activity (Fig. 3b). The maximum water permeabilities for **1**-**5** are all achieved at a lipid/channel molar ratio of 4200:1 within the tested range (3000:1 to 5400:1). At this ratio, **1** achieves a water permeability of 5.66 ± 0.67 × 10^{-14} cm^3/s, corresponding to of 1.8 × 10^9 H_2O s^{-1} per channel. This value is 2.9 times that of gramicidin A (gA)[33] and about 60% of the channel **A**'s permeability. For pentamer **2**, which has a reduced pore size of 2.2 Å (Fig. 2d), the water permeability decreases to 2.74 ± 0.28 × 10^{-14} cm^3/s or 0.87 × 10^9 H_2O s^{-1} per channel. Interestingly, although hybrid pentamer **5** has a larger pore size of 2.4 Å compared to **2** (Fig. 2e), its water permeability was lower, measuring 1.99 ± 0.28 × 10^{-14} cm^3/s (0.87 × 10^9 H_2O s^{-1} per channel). This reduced activity can be attributed to the interdigitation of two self-assembled 1D nanotubes during 2D stacking, which effectively narrows the pore size and limits transmembrane water transport. While the crystal structure of **3** was not obtained, its water permeability was found to be 1.14 × 10^9 H_2O s^{-1} per channel, suggesting it likely also forms a self-assembled 1D nanotube similar to **1** and **2**. The water permeability of **4** was determined to be 0.75 × 10^9 H_2O s^{-1} per channel, positioning it between the values for **2** and **5** and similarly indicating its ability to self-assemble into 1D nanotubes.

Using Arrhenius plots of water permeability as a function of temperature, we determined the activation energy (E_a) for water to enter the pore to be 11.67 ± 0.24 kcal/mol for channel **1** (Fig. S3). This value is only slightly lower than that of the DOPC liposome (12.56 ± 0.11 kcal/mol) and channel **A** (12.06 ± 0.11 kcal/mol). The small difference of 3% in the E_a value between **1** and **A** suggests the water dehydration penalty at the channel entrance has a negligible impact on the observed approximately twofold difference in water flow rate between **1** and **A**. Notably, an activation energy of 11.67 kcal/mol seems excessively high for a superfast water conductor such as **1**, particularly compared to the E_a value of 5.1 kcal/mol for AQP1, which transports 5.9 × 10^9 H_2O s^{-1} per channel. The relative importance of

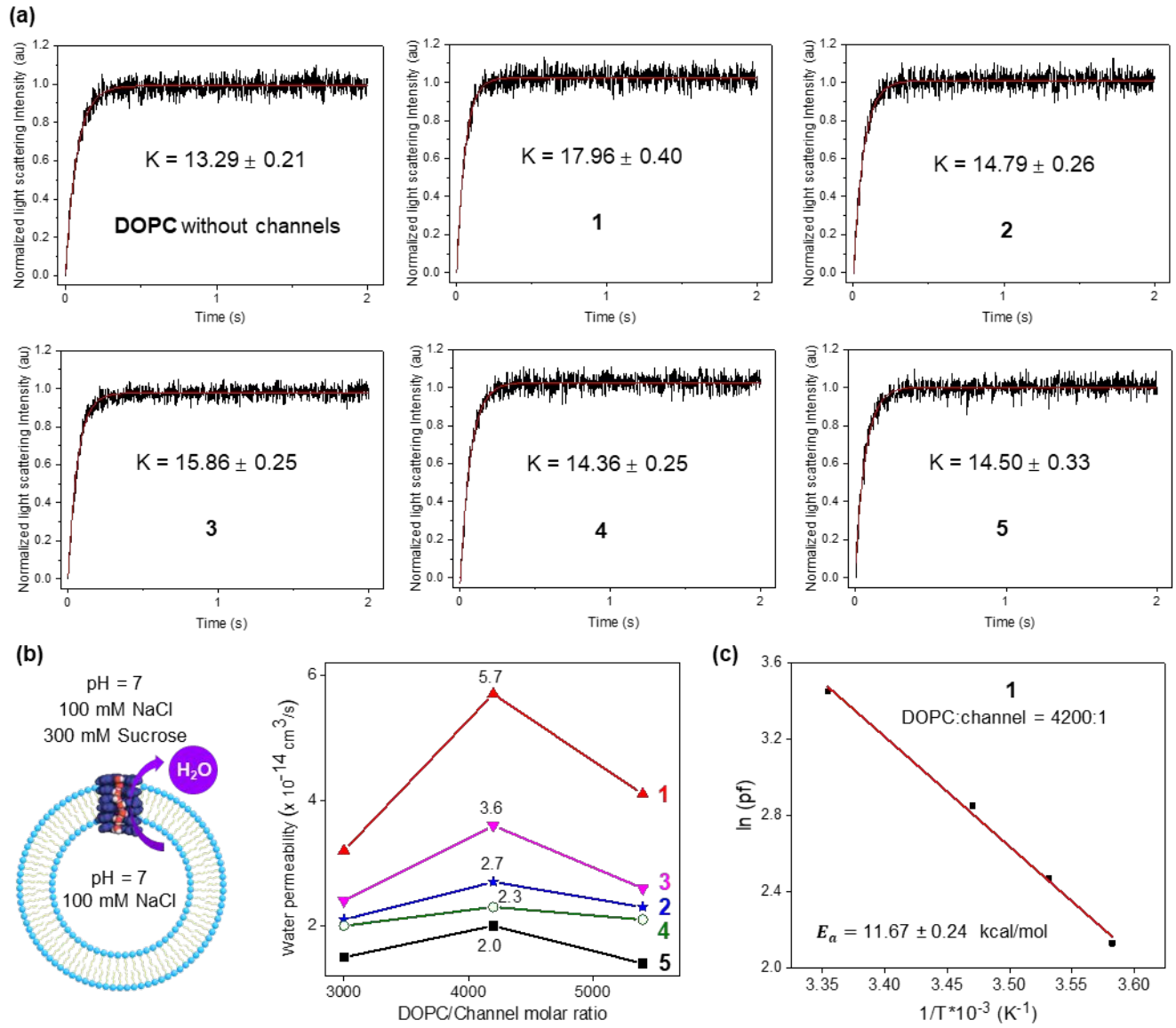

Fig.3 Water transport properties of pentamers **1-5**. (a) Representative water transport curves for DOPC only and **1-5** obtained using a stopped flow apparatus at a lipid/channel molar ratio of 4200:1. Exponential coefficients (K) were obtained by fitting the data into the equation of $y = A\exp(-kx) + y0$. (b) LUV-based hypertonic conditions (300 mM sucrose) for water permeability measurement for **1-5** at different lipid/channel molar ratios, with data averaged in triplicate. (c) Arrhenius plots of the water permeability as a function of temperature (at 6-25 °C) for **1** for determining activation energies (E_a) averaged over three runs. DOPC = 1,2-dioleoyl-sn-glycero-3-phosphocholine.

pore surface wettability (e.g., the ability of channel-lining residues to form H-bonds with water molecules) and positive charges near the pore entrance[52] appears to be insignificant in our current water channel system, making it difficult to explain the differential water flow rates between **1** and **A**. Based on our previous work, we suggest that the enhanced water transport mediated by channel **A**, compared to channel **1**, is primarily due to the increased freedom of water molecules and/or a significantly reduced deviation from the optimal hydrogen-bonded structure, both resulting from the enlarged pore seen in **A**.

High Selectivity in Pentamer 1-Mediated Water Transport

Fast water transport is only one feature of naturally occurring aquaporin AqpZ; its high selectivity in water transport is equally significant, as it effectively rejects both salts (NaCl and KCl) and protons. For practical applications in water purification, high selectivity may be as crucial, if not more so, as the rate of water transport. To investigate the selectivity of hybrid pentamer-mediated water transport, we designed a series of lipid bilayer experiments. Using EYPC-based large unilamellar vesicles (LUVs) and the pH-sensitive HPTS assay, we measured the fractional ion transport activities of pentamers **1-5**, which were found to increase in the order of **5** < **4** < **3** < **2** < **1** (Fig. 4a). The results demonstrated that the ion transport activities of **1-5** were independent of the presence of MCl, indicating that they were unable to transport cations such as Na^+ or

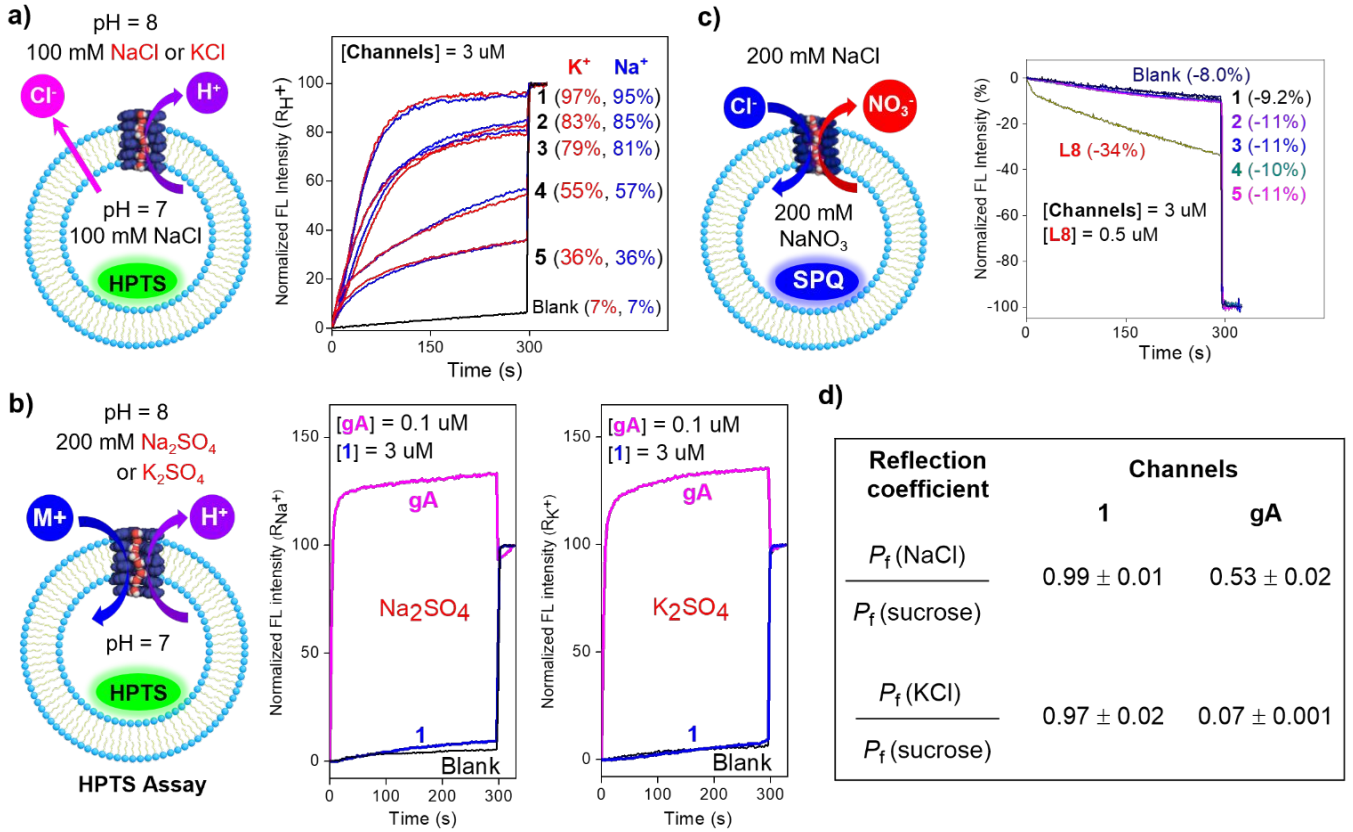

Reflection coefficient	Channels 1	gA
$\frac{P_f\,(NaCl)}{P_f\,(sucrose)}$	0.99 ± 0.01	0.53 ± 0.02
$\frac{P_f\,(KCl)}{P_f\,(sucrose)}$	0.97 ± 0.02	0.07 ± 0.001

Fig. 4 Water permeability of channels **1-5**. (a) The pH-sensitive HPTS assay for assessing ion-transport activities of channels **1-5** in EYPC-based LUVs. (b) HPTS-based LUV assays under high ionic concentration gradients, confirming that **1** does not transport both Na^+ and K^+ ions. (c) SPQ-based LUV assay, confirming that channel channel **1**, **2**, **3**, **4** and **5** do not transport Cl^- anions. (d) Water permeability measured using three types of hypertonic conditions (300 mM sucrose, 150 mM NaCl, or 150 mM KCl), indicating complete salt rejection by **1** and incomplete salt rejection by gA. HPTS = 8-Hydroxypyrene-1,3,6-trisulfonic acid trisodium salt; SPQ = 6-methoxy-N-(3-sulfopropyl)-quinolinium.

K^+. The most likely species to be transported across the membrane is either anion or proton.

To further confirm that these hybrid pentamers do not transport Na^+ and K^+ ions, we applied high metal sulphate concentration gradients (200 mM Na_2SO_4 or K_2SO_4, Fig. 4b) to evaluate the activities of **1** and gA. Gramicidin A showed rapid increases in fluorescence intensity, exceeding 120% within 10 seconds at a concentration of 0.1 μM ([gA channel] = 0.05 μM). In contrast, **1** exhibited negligible changes of less than 3% at a concentration of 3 μM ([channel] = 0.5 μM) for both Na^+ and K^+ ions. This clearly indicates that neither Na^+ nor K^+ ion could permeate the pore formed by **1**.

Using the chloride-sensitive SPQ assay[54], we observed rapid quenching of the SPQ dye by chloride channel **L8** [53] at a concentration of 0.5 μM ([channel] = 0.1 μM), but not by **1** at five times the concentration of **L8** (Fig. 4c). This finding excludes Cl^- anions as transportable species by **1**.

Unlike gA, which can transport Na^+, K^+, and H^+ ions, **1** does not transport Na^+ or Cl^- ions. Consequently, to satisfy the charge neutrality of the system, the efflux of protons through **1** as observed in Fig. 4a can only be accompanied by the slower passive diffusion of Cl^- anions across the membrane, rather than through the fast, channel-mediated transport. A highly active proton carrier, FCCP (carbonyl cyanide 4-(trifluoromethoxy)phenylhydrazone), was used to verify the H^+/Cl^- symport mechanism using the same HPTS assay shown in Fig. 4a. In the presence of FCCP, there was no enhancement of transport activity by **1**, suggesting that **1** could only transport protons, with the passive diffusion of Cl^- anions as the rate-limiting step. (Fig. S4).

We compared the water permeability (P_f) values of vesicles under three different hypertonic conditions: 300 mM sucrose (non-permeable), 150 mM NaCl, and 150 mM KCl (Fig. 4d). For channel **1**, the average P_f values (measured in triplicate) at a lipid/channel ratio of 4200:1 are 145.48 ± 3.25 μm/s for sucrose, 144.51 ± 4.41 μm/s for NaCl, and 141.20 ± 5.57 μm/s for KCl. The reflection coefficients, defined as the ratio of the P_f value for salt to that for sucrose, are0.99 ± 0.01 for NaCl and 0.97 ± 0.02 for KCl. These reflection coefficients, which are insignificantly different from 1.00, confirm that **1** achieves a high rejection of both NaCl and KCl due to the narrow size of its aquapore (2.8 Å), which is sufficient only for a single water molecule, and its lack of binding sites for freeing ions from their hydration shells. For comparison, gA exhibits reflection coefficients of 0.53 ± 0.02 for NaCl and 0.07 ± 0.001 for KCl,[33] highlighting its high permeability toward Na^+ and K^+ ions. This is in stark contrast to the high salt rejection capacity of **1**.

Computational Estimation of Transport Selectivities of Water/Na^+, Water/K^+, and Water/Cl^-

We further conducted a computational study of a 2000 ns trajectory to gain additional insights into the selectivity of **1**-mediated transport for water over Na^+, K^+, and Cl^- (Fig.5, Table 1 and Fig. S9). For evaluating water/Na^+ selectivity, the simulation setup included 10000 water molecules and 110 NaCl. Over the 2000 ns period, 811 water molecules successfully passed through the channel, corresponding to a flux of 4.1×10^8 water molecules per second. Additionally, 25660 water molecules entered at least 1/16 of the channel length (~2 Å). During this period, no ions (Na^+ or Cl^-) were observed to enter or remain in the channel at any time. Based on these results, the estimated water/NaCl selectivity is at least 282 (= 25660/(10000/110)).

For water/K^+ selectivity, the simulation setup also included 10000 water molecules but with 110 KCl. Over the same 2000 ns period, 850 water molecules passed through the channel, equivalent to a flux of 4.3×10^8 water molecules per second, and 24710 water molecules entered at least 1/16 of the channel length (~2 Å). Similarly, no ions (K^+ or Cl^-) were detected inside the channel at any time. The estimated water/KCl selectivity is at least 272 (= 24710/(10000/110)).

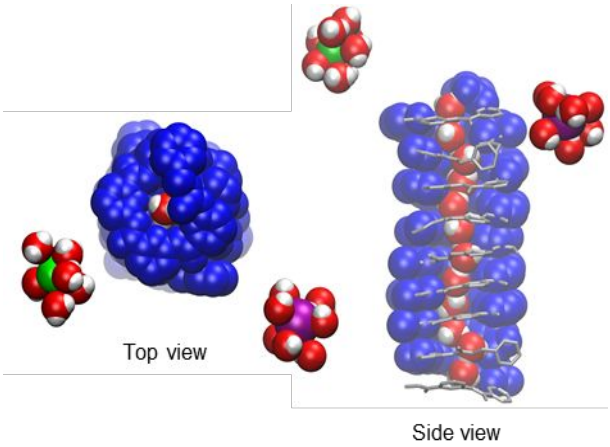

Fig. 5. Top and side views of a representative snapshot from MD-simulated structures, revealing the formation of H-bonded 1D water chain and hydrated K^+ (green) and Na^+ (purple) ions near the pore entry. Ions are blocked because the channel pore size is small, which requires the energetically costly stripping of the ion's solvation shell. For the movie illustrating how a water molecule transports through the channel, see Fig. S9.

Table 1. Computational estimation of water transport speed and selectivity through channel 1[a]

	no. of water molecules that passed the channel	Water transport speed (H_2O/s)	no. of water molecules that entered 1/16 of the channel (about 2 Å)	Selectivity (water/MCl)
NaCl system	811	4.1×10^8	25660	282[b]
KCl system	850	4.3×10^8	24710	272[c]

[a] The simulation setup box contains 110 NaCl or 110 KCl dissolved in 10000 water molecules (~0.6 M MCl, M = Na or K). For both NaCl and KCl systems, the simulation was run for 2000 ns. [b] Value = 25660/(10000/110). [c] Value = 24710/(10000/110)

These remarkably high selectivities for water over Na^+, K^+, and Cl^- align well with expectations. As previously discussed, the narrow hollow cavity of approximately 2.8 Å in **1** is just large enough to accommodate a single water molecule (Fig.5 and Fig. S9). This structural constraint, combined with the absence of binding elements in **1** to compensate for the dehydration energy required for ions to enter the channel, prevents their entry and passage through the channel in a mostly dehydrated state.

Conclusions

In summary, we designed and synthesized hybrid pentamers **1**-**5** incorporating a non-helicity codon (e.g., a phenyl group) that nevertheless still enables the folding of partially H-bonded aromatic foldamers into a helical structure. These helical structures further self-assemble into 1D nanotubes with pore sizes of 2.2–2.8 Å via a "sticky-end"-mediated assembly strategy developed by us, facilitating superfast transmembrane water transport on the order of 10^9 H_2O s^{-1} per channel. The position of the incorporated phenyl group regulates the pore size through steric hindrance caused by its protruding hydrogen atoms. Additionally, the inability of the phenyl group to form hydrogen bonds with adjacent amide N–H bonds alters the stacking arrangement of the hybrid pentamers. These structural variations result in a threefold difference in water transport capacity among the five hybrid pentamers. Notably, pentamer **1** demonstrates an impressive water transport rate of 1.8 x 10^9 H_2O s^{-1} per channel and high salt rejection, indicating its potential for applications in fabricating novel biomimetic reverse osmosis membranes. This advancement could contribute to the development of low-energy, highly efficient water purification systems.

Conflicts of interest

There are no conflicts to declare.

Acknowledgements

This work is supported by the National Natural Science Foundation of China (22271049 and 22371048), NSF (CHE-2205220 (Z. Liu)), Natural Science Foundation of Fujian Province (2023J01054) and a start-up grant from Fuzhou University.

References

1. M. M. Mekonnen and A. Y. Hoekstra, Four billion people facing severe water scarcity, *Sci. Adv.*, 2016, ***2***, e1500323.
2. C. Y. Tang; Z. Yang; H. Guo; J. J. Wen; L. D. Nghiem and E. Cornelissen, Potable Water Reuse through Advanced Membrane Technology, *Environ. Sci. Technol.*, 2018, ***52***, 10215-10223.
3. J. Eliasson, The rising pressure of global water shortages, *Nature*, 2015, ***517***, 6.
4. C. J. Porter; J. R. Werber; M. Zhong; C. J. Wilson and M. Elimelech, Pathways and Challenges for Biomimetic Desalination Membranes with Sub-Nanometer Channels, *ACS. Nano*, 2020, ***14***, 10894-10916.
5. R. J. Petersen, Composite Reverse-Osmosis and Nanofiltration Membranes, *J Membrane Sci*, 1993, ***83***, 81-150.

6. L. F. Greenlee; D. F. Lawler; B. D. Freeman; B. Marrot and P. Moulin, Reverse osmosis desalination: water sources, technology, and today's challenges, *Water Res*, 2009, ***43***, 2317-2348.
7. J. Imbrogno and G. Belfort, Membrane Desalination: Where Are We, and What Can We Learn from Fundamentals?, *Annu. Rev. Chem. Biomol.*, 2016, ***7***, 29-64.
8. K. Murata; K. Mitsuoka; T. Hirai; T. Walz; P. Agre; J. B. Heymann; A. Engel and Y. Fujiyoshi, Structural determinants of water permeation through aquaporin-1, *Nature*, 2000, ***407***, 599-605.
9. E. Tajkhorshid; P. Nollert; M. O. Jensen; L. J. Miercke; J. O'Connell; R. M. Stroud and K. Schulten, Control of the selectivity of the aquaporin water channel family by global orientational tuning, *Science*, 2002, ***296***, 525-530.
10. K. Takata; T. Matsuzaki and Y. Tajika, Aquaporins: water channel proteins of the cell membrane, *Prog Histochem Cytochem*, 2004, ***39***, 1-83.
11. M. J. Borgnia; D. Kozono; G. Calamita; P. C. Maloney and P. Agre, Functional reconstitution and characterization of AqpZ, the E. coli water channel protein, *J Mol Biol*, 1999, ***291***, 1169-1179.
12. B. Gong, Artificial water channels: inspiration, progress, and challenges, *Faraday Discuss.*, 2018, ***209***, 415-427.
13. M. Elimelech and W. A. Phillip, The future of seawater desalination: energy, technology, and the environment, *Science*, 2011, ***333***, 712-717.
14. M. Barboiu and A. Gilles, From natural to bioassisted and biomimetic artificial water channel systems, *Acc. Chem. Res.*, 2013, ***46***, 2814-2823.
15. A. G. Fane; R. Wang and M. X. Hu, Synthetic membranes for water purification: status and future, *Angew. Chem., Int. Ed.*, 2015, ***54***, 3368-3386.
16. Y. Huo and H. Q. Zeng, "Sticky"-Ends-Guided Creation of Functional Hollow Nanopores for Guest Encapsulation and Water Transport, *Acc. Chem. Res.*, 2016, ***49***, 922-930.
17. J. R. Werber; C. O. Osuji and M. Elimelech, Materials for next-generation desalination and water purification membranes, *Nat. Rev. Mater.*, 2016, ***1***, 16018.
18. J. R. Werber and M. Elimelech, Permselectivity limits of biomimetic desalination membranes, *Sci. Adv.*, 2018, ***4***, eaar8266.
19. W. Song and M. Kumar, Artificial water channels: toward and beyond desalination, *Curr. Opin. Chem. Eng.*, 2019, ***25***, 9-17.
20. P. Wagh and I. C. Escobar, Biomimetic and bioinspired membranes for water purification: A critical review and future directions, *Environ. Prog. Sustain.*, 2019, ***38***, e13215.
21. Y. Le Duc; M. Michau; A. Gilles; V. Gence; Y. M. Legrand; A. van der Lee; S. Tingry and M. Barboiu, Imidazole-quartet water and proton dipolar channels, *Angew. Chem., Int. Ed.*, 2011, ***50***, 11366-11372.
22. X. B. Hu; Z. Chen; G. Tang; J. L. Hou and Z. T. Li, Single-molecular artificial transmembrane water channels, *J. Am. Chem. Soc.*, 2012, ***134***, 8384-8387.
23. X. Zhou; G. Liu; K. Yamato; Y. Shen; R. Cheng; X. Wei; W. Bai; Y. Gao; H. Li; Y. Liu; F. Liu; D. M. Czajkowsky; J. Wang; M. J. Dabney; Z. Cai; J. Hu; F. V. Bright; L. He; X. C. Zeng; Z. Shao and B. Gong, Self-assembling subnanometer pores with unusual mass-transport properties, *Nat. Commun.*, 2012, ***3***, 949.
24. H. Zhao; S. Sheng; Y. Hong and H. Q. Zeng, Proton gradient-induced water transport mediated by water wires inside narrow aquapores of aquafoldamer molecules, *J. Am. Chem. Soc.*, 2014, ***136***, 14270-14276.
25. W. Si; P. Xin; Z. T. Li and J. L. Hou, Tubular Unimolecular Transmembrane Channels: Construction Strategy and Transport Activities, *Acc. Chem. Res.*, 2015, ***48***, 1612-1619.
26. Y. X. Shen; W. Si; M. Erbakan; K. Decker; R. De Zorzi; P. O. Saboe; Y. J. Kang; S. Majd; P. J. Butler; T. Walz; A. Aksimentiev; J. L. Hou and M. Kumar, Highly permeable artificial water channels that can self-assemble into two-dimensional arrays, *Proc. Natl. Acad. Sci. U.S.A.*, 2015, ***112***, 9810-9815.
27. E. Licsandru; I. Kocsis; Y. X. Shen; S. Murail; Y. M. Legrand; A. van der Lee; D. Tsai; M. Baaden; M. Kumar and M. Barboiu, Salt-Excluding Artificial Water Channels Exhibiting Enhanced Dipolar Water and Proton Translocation, *J. Am. Chem. Soc.*, 2016, ***138***, 5403-5409.
28. R. H. Tunuguntla; R. Y. Henley; Y. C. Yao; T. A. Pham; M. Wanunu and A. Noy, Enhanced water permeability and tunable ion selectivity in subnanometer carbon nanotube porins, *Science*, 2017, ***357***, 792-796.
29. X. Kong; Z. Zhao and J. Jiang, Dipeptides Embedded in a Lipid Bilayer Membrane as Synthetic Water Channels, *Langmuir*, 2017, ***33***, 11490-11495.
30. C. Helix-Nielsen, Biomimetic Membranes as a Technology Platform: Challenges and Opportunities, *Membranes*, 2018, ***8*** , 44.
31. I. Kocsis; M. Sorci; H. Vanselous; S. Murail; S. E. Sanders; E. Licsandru; Y. M. Legrand; A. van der Lee; M. Baaden; P. B. Petersen; G. Belfort and M. Barboiu, Oriented chiral water wires in artificial transmembrane channels, *Sci. Adv.*, 2018, ***4***, eaao5603.
32. Z. J. Yan; D. Wang; Z. Ye; T. Fan; G. Wu; L. Deng; L. Yang; B. Li; J. Liu; T. Ma; C. Dong; Z. T. Li; L. Xiao; Y. Wang; W. Wang and J. L. Hou, Artificial Aquaporin That Restores Wound Healing of Impaired Cells, *J. Am. Chem. Soc.*, 2020, ***142***, 15638-15643.
33. J. Shen; R. Ye; A. Romanies; A. Roy; F. Chen; C. Ren; Z. Liu and H. Q. Zeng, Aquafoldmer-Based Aquaporin-like Synthetic Water Channel, *J. Am. Chem. Soc.*, 2020, ***142***, 10050-10058.
34. J. Chen; Q. Li; P. Wu; J. Liu; D. Wang; X. Yuan; R. Zheng; R. Sun and L. Li, Cyclic gamma-Peptides With Transmembrane Water Channel Properties, *Front. Chem.*, 2020, ***8***, 368.
35. J. Shen; J. Fan; R. Ye; N. Li; Y. Mu and H. Q. Zeng, Polypyridine-Based Helical Amide Foldamer Channels: Rapid Transport of Water and Protons with High Ion Rejection, *Angew. Chem., Int. Ed.*, 2020, ***59***, 13328-13334.
36. W. Song; H. Joshi; R. Chowdhury; J. S. Najem; Y.-x. Shen; C. Lang; C. B. Henderson; Y.-M. Tu; M. Farell; M. E. Pitz; C. D. Maranas; P. S. Cremer; R. J. Hickey; S. A. Sarles; J.-l. Hou; A. Aksimentiev and M. Kumar, Artificial water channels enable fast and selective water permeation through water-wire networks, *Nat. Nanotechnol.*, 2020, ***15***, 73-79.
37. E. Abaie; L. M. M. Xu and Y. X. Shen, Bioinspired and biomimetic membranes for water purification and chemical separation: A review, *Front. Env. Sci. Eng.*, 2021, ***15***.
38. G. Goel; C. Hélix-Nielsen; H. M. Upadhyaya and S. Goel, A bibliometric study on biomimetic and bioinspired membranes for water filtration, *npj Clean Water*, 2021, ***4***, 41.
39. L. B. Huang; M. Di Vincenzo; Y. Li and M. Barboiu, Artificial Water Channels: Towards Biomimetic Membranes for Desalination, *Chemistry*, 2021, ***27***, 2224-2239.
40. M. Di Vincenzo; A. Tiraferri; V. E. Musteata; S. Chisca; M. Deleanu; F. Ricceri; D. Cot; S. P. Nunes and M. Barboiu, Tunable membranes incorporating artificial water channels for high-performance brackish/low-salinity water reverse osmosis

desalination, *Proc. Natl. Acad. Sci. U.S.A.*, 2021, ***118***, e2022200118.
41. Y. Shen; F. Fei; Y. Zhong; C. Fan; J. Sun; J. Hu; B. Gong; D. M. Czajkowsky and Z. Shao, Controlling Water Flow through a Synthetic Nanopore with Permeable Cations, *ACS Cent. Sci.*, 2021, ***7***, 2092-2098.
42. A. Roy; J. Shen; H. Joshi; W. Song; Y. M. Tu; R. Chowdhury; R. Ye; N. Li; C. Ren; M. Kumar; A. Aksimentiev and H. Q. Zeng, Foldamer-based ultrapermeable and highly selective artificial water channels that exclude protons, *Nat. Nanotechnol.*, 2021, ***16***, 911-917.
43. Y. J. Lim; K. Goh and R. Wang, The coming of age of water channels for separation membranes: from biological to biomimetic to synthetic, *Chem. Soc. Rev.*, 2022, ***51***, 4537-4582.
44. L. Shen; R. Cheng; M. Yi; W. S. Hung; S. Japip; L. Tian; X. Zhang; S. Jiang; S. Li and Y. Wang, Polyamide-based membranes with structural homogeneity for ultrafast molecular sieving, *Nat. Commun.*, 2022, ***13***, 500.
45. F. Zhou; J. Lee; R. Wang and H. Su, Mechanisms of Efficient Desalination by a Two-Dimensional Porous Nanosheet Prepared via Bottom-Up Assembly of Cucurbit[6]urils, *Membranes*, 2022, ***12*** ,252.
46. J. Shen; A. Roy; H. Joshi; L. Samineni; R. Ye; Y. M. Tu; W. Song; M. Skiles; M. Kumar; A. Aksimentiev and H. Q. Zeng, Fluorofoldamer-Based Salt- and Proton-Rejecting Artificial Water Channels for Ultrafast Water Transport, *Nano Lett*, 2022, ***22***, 4831-4838.
47. I. M. Andrei; W. Chen; M. Baaden; S. P. Vincent and M. Barboiu, Proton- versus Cation-Selective Transport of Saccharide Rim-Appended Pillar[5]arene Artificial Water Channels, *J. Am. Chem. Soc.*, 2023, ***145***, 21904-21914.
48. Q. Xiao; T. Fan; Y. L. Wang; Z. T. Li; J. L. Hou and Y. F. Wang, Artificial Water Channel that Couples with Cell Protrusion Formation, *CCS Chem.*, 2023, ***5***, 1745-1752.
49. C. Dutta; P. Krishnamurthy; D. D. Su; S. H. Yoo; G. W. Collie; M. Pasco; J. K. Marzinek; P. J. Bond; C. Verma; A. Grélard; A. Loquet; J. W. Li; M. Luo; M. Barboiu; G. Guichard; R. M. Kini and P. P. Kumar, Nature-inspired synthetic oligourea foldamer channels allow water transport with high salt rejection, *Chem*, 2023, ***9***, 2237-2254.
50. Y. Itoh; S. Chen; R. Hirahara; T. Konda; T. Aoki; T. Ueda; I. Shimada; J. J. Cannon; C. Shao; J. Shiomi; K. V. Tabata; H. Noji; K. Sato and T. Aida, Ultrafast water permeation through nanochannels with a densely fluorous interior surface, *Science*, 2022, ***376***, 738-743.
51. H. Q. Zhao; W. Q. Ong; F. Zhou; X. Fang; X. Y. Chen; S. F. Y. Li; H. B. Su; N. J. Cho and H. Q. Zeng, Chiral crystallization of aromatic helical foldamers complementarities in shape and end functionalities, *Chem. Sci.*, 2012, ***3***, 2042-2046.
52. A. Horner; F. Zocher; J. Preiner; N. Ollinger; C. Siligan; S. A. Akimov and P. Pohl, The mobility of single-file water molecules is governed by the number of H-bonds they may form with channel-lining residues, *Sci. Adv.*, 2015, ***1***, e1400083.
53. C. Ren; X. Ding; A. Roy; J. Shen; S. Zhou; F. Chen; S. F. Yau Li; H. Ren; Y. Y. Yang and H. Q. Zeng, A halogen bond-mediated highly active artificial chloride channel with high anticancer activity, *Chem Sci*, 2018, ***9***, 4044-4051.
54. A. S. Verkman; R. Takla; B. Sefton; C. Basbaum and J. H. Widdicombe, Quantitative fluorescence measurement of chloride transport mechanisms in phospholipid vesicles, *Biochemistry*, 1989, ***28***, 4240-4244.

Data availability statement:

All relevant data are within the manuscript and its Supplementary Information.